Available online at www.sciencedirect.com
ScienceDirect
Trans. Nonferrous Met. Soc. China 25(2015) 850−855
Transactions of Nonferrous Metals Society of China
www.tnmsc.cn

Effects of Co and Al addition on martensitic transformation and microstructure in ZrCu-based shape memory alloys

Wei-hong GAO, Xiang-long MENG, Wei CAI, Lian-cheng ZHAO

School of Materials Science and Engineering, Harbin Institute of Technology, Harbin 150001, China

Received 21 March 2014; accepted 24 July 2014

Abstract: The effect of ternary alloying element Al and quaternary alloying element Co on the martensitic transformation of ZrCu-based shape memory alloy was investigated. The results show that the addition of Al and Co in ZrCu alloy decreases both the martensitic transformation temperature and the martensitic transformation temperature hysteresis. Transmission electron microscope (TEM) observations reveal that the *Cm* martensite structure is the preferential formation phase. The intervariant structures in ZrCuAlCo alloy are (021) type I twins, while the dominant substructures inside the martensite variant are the (001) compound twins. With the increase of Co content, tensile fracture strength and strain are improved obviously.

Key words: ZrCu-based alloy; shape memory alloy; martensitic transformation; microstructure

1 Introduction

ZrCu-based shape memory alloys (SEA) have attracted considerable attention in recent years due to their potentialities for high temperature shape memory alloys as well as for metallic glasses with high ductility properties [1−4]. Recent advancements in ZrCu-based alloys come at the intersection between shape memory alloys and metallic glasses [5−7]. For $Zr_{48}Cu_{47.5}Al_4Co_{0.5}$ bulk metallic glass composites, the strain hardening rate was enhanced and plastic instability was suppressed due to a martensitic transformation (MT) of *B*2 to *B*19′ which is associated with shape memory effect [8]. However, there are some reports about how to improve the glass-forming ability and the mechanical properties [9]. Few reports about the MT behavior in ZrCu intermetallic compound are given. In fact, the SME in ZrCu intermetallic (only about 3%) is associated with a MT from a *B*2 type structure to two monoclinic martensitic structures: one with a base structure (*B*19′) with *P*2/*m* symmetry and the other with a superstructure with *Cm* symmetry [10,11]. In addition, the transformation temperature hysteresis of ZrCu-based SMA is large and the thermal stability of ZrCu-based SMA is poor [12]. However, it is not clear that how the addition of different alloying elements to ZrCu is linked with the martensitic transformation and the microstructure [13−18].

In the present work, the influences of Al and Co addition of the ZrCuAlCo quaternary high temperature SMAs on the microstructure, the phase transformation behaviors and mechanical properties were investigated by X-ray diffraction (XRD), transmission electron microscopy (TEM) observation, differential scanning calorimeter (DSC) measurement, tensile tests and scanning electron microscopy (SEM). The further explanations from microstructure on martensite transformation temperature and mechanical properties were discussed.

2 Experimental

The $Zr_{48}Cu_{47.5}Al_4Co_{0.5}$, $Zr_{47.5}Cu_{46.5}Al_5Co_1$ and $Zr_{47.5}Cu_{45.5}Al_5Co_2$ alloys were prepared by arc-melting using high-purity metals (99.99%) of Cu, Zr, Al and Co in an induction furnace under argon atmosphere. The ingots were then remelted six times to ensure the composition homogeneity (each time turning the button 180°). The samples were annealed in vacuum quartz tubes at 800 °C for 4 h, followed by water-quenching.

Foundation item: Projects (51171052, 51171052, 51322102) supported by the National Natural Science Foundation of China; Projects (2011CB012904, 2012CB619400) supported by the National Basic Research Program of China; Project (20112302130006) supported by Doctoral Program Foundation of Institutions of Higher Education of China; Project (HIT. BRET III 201201) supported by the Fundamental Research Funds for the Central Universities, China
Corresponding author: Xiang-long MENG; Tel: +86-451-86418649; Fax: +86-451-86415038; E-mail: xlmeng@hit.edu.cn
DOI: 10.1016/S1003-6326(15)63673-1

The plates with 1 mm in thickness were cut from the ingot by wire-electrode cutting, then ground and polished. Samples for transmission electron microscopy (TEM) observations were obtained by punching 3 mm-diameter samples from the plates and mechanically polishing them to a thickness of 20 μm. The TEM samples were prepared by double-jet electro-polishing in an electrolyte solution consisting of 70% (volume fraction) methanol and 30% (volume fraction) nitri cacid at 253 K. TEM observations were performed with a Philips Tecnai-G^2 F30 electron microscope operated at 300 kV. XRD measurements were carried out at room temperature with Cu K_α radiation. The phase transformation temperatures of the alloy were determined by a differential scanning calorimeter (DSC) with a PERKINELMER DSC8000 calorimeter. Heating/cooling scans were undertaken in the temperatures range of −100 to 600 K with a rate of 20 K/min. The tensile tests were performed at room temperature on an Instron 5569 testing system at a crosshead displacement speed of 0.2 mm/min. The microstructure of the alloys was examined with a Quanta 200FEG scanning electron microscope (SEM).

3 Results and discussion

Figure 1 shows the optical micrographs of as-cast ZrCuAlCo alloys, and the sampling position of every ingot is the same. It can be observed from Fig. 1 that with the increase of Co content the grain size becomes small. The average grain sizes of $Zr_{48}Cu_{47.5}Al_4Co_{0.5}$, $Zr_{47.5}Cu_{46.5}Al_5Co_1$, and $Zr_{47.5}Cu_{45.5}Al_5Co_2$ alloys are about 10, 8 and 6 μm, respectively. The decomposed phases appear along the grain boundary. Figure 2 shows the XRD patterns of ZrCuAlCo alloys. The analysis of the diffraction patterns reveals that the patterns of the alloys are different. The reflections in patterns for $Zr_{48}Cu_{47.5}Al_4Co_{0.5}$ and $Zr_{47.5}Cu_{46.5}Al_5Co_1$ alloys are indexed with the co-existence of *B*19′ and *Cm* martensite, the low-temperature equilibrium phases $Cu_{10}Zr_7$ and $CuZr_2$. The reflections in patterns for $Zr_{47.5}Cu_{45.5}Al_5Co_2$ alloy are indexed with Co_2Zr_3 and *B*2 phases. The XRD results indicate that the small Co alloying variation in the Zr/Cu ratio changes the crystal structure of the phases from martensite to austenite at room temperature in this alloy series.

Figure 3 shows the TEM bright-field (BF) micrographs and selected area electron diffraction (SAED) patterns of ZrCuAlCo alloys. The thermal martensite variants exhibit self-accommodation morphology. The typical bright field image exhibits large spear-like and plate-like variants with 400 nm in width, and the hair-like stripes can be seen in big plate, as shown in Fig. 3(a). The martensite variants are found to

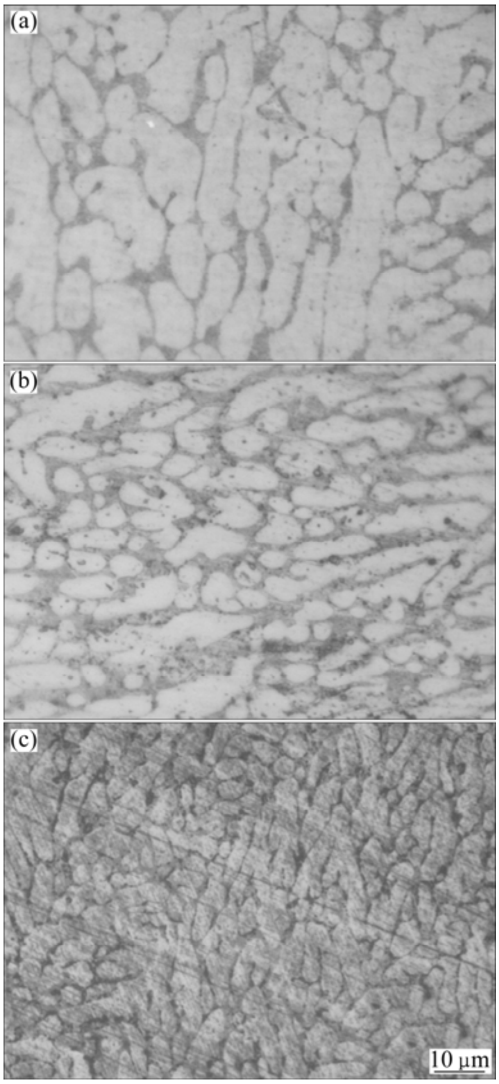

Fig. 1 Optical micrographs of as-cast ZrCuAlCo alloys: (a) $Zr_{48}Cu_{47.5}Al_4Co_{0.5}$; (b) $Zr_{47.5}Cu_{46.5}Al_5Co_1$; (c) $Zr_{47.5}Cu_{45.5}Al_5Co_2$

be (021) type I twin related, as clearly indicated by the corresponding electron diffraction patterns (EDPs) as shown in Fig. 3(b). The substructure is (001) compound twin by indexing the corresponding EDPs, as shown in Fig. 3(c). The morphologies of $Zr_{47.5}Cu_{46.5}Al_5Co_1$ alloy shown in Fig. 3(d) do not change obviously except for the width of the plate narrower. It is found that very fine microtwins with the thickness of several nanometers exist in the interior of the martensite variant, while they start and end in the interior of a martensite variant. The relationship between the martensite variants does not change, as shown in Fig. 3(e). Figure 3(f) shows the TEM image of the $Zr_{47.5}Cu_{45.5}Al_5Co_2$ alloy. The microstructures are different obviously. It is found that both of the austenite and the martensite coexist as marked by *A* and *M* with the corresponding EDPs shown in Figs. 3(g) and (h), respectively. This means that the austenite is stable in a wider temperature range by

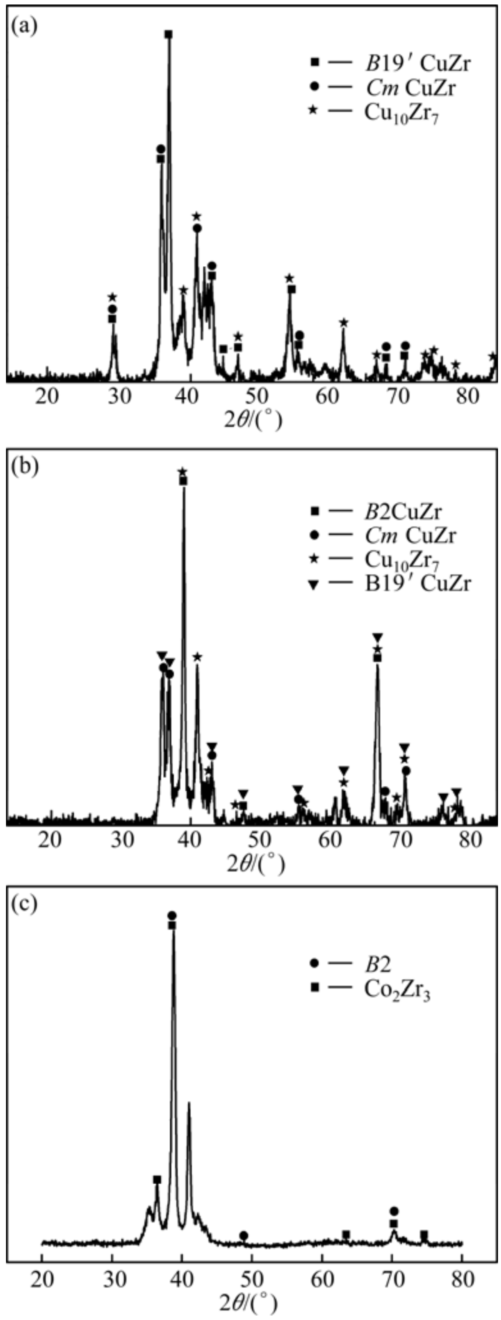

Fig. 2 XRD patterns of as-cast ZrCuAlCo alloys: (a) $Zr_{48}Cu_{47.5}Al_4Co_{0.5}$; (b) $Zr_{47.5}Cu_{46.5}Al_5Co_1$; (c) $Zr_{47.5}Cu_{45.5}Al_5Co_2$

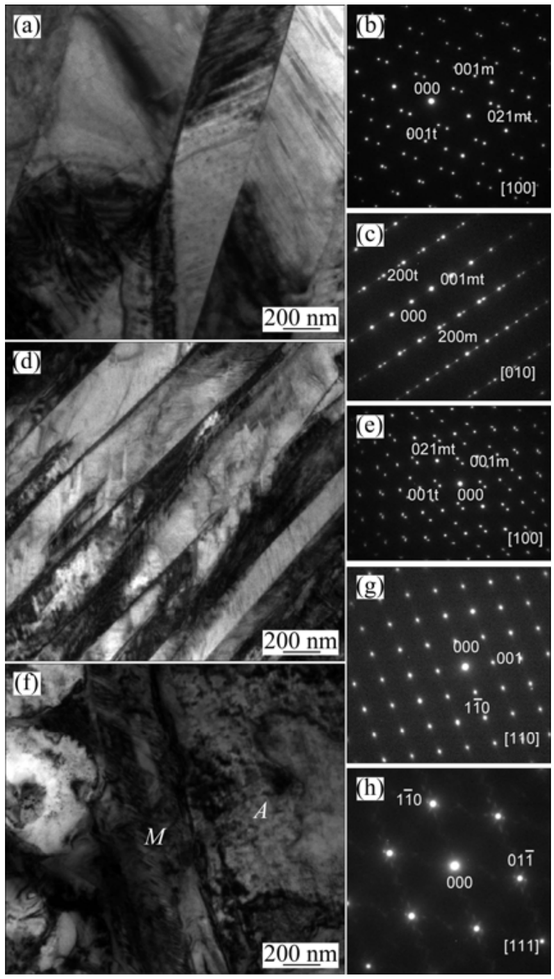

Fig. 3 TEM images of ZrCuAlCo alloys and corresponding SAED patterns: (a) Bright field image of $Zr_{48}Cu_{47.5}Al_4Co_{0.5}$ alloy; (b, c) SAED patterns taken from intervariant and substructures inside martensite variant in (a); (d) Bright field image of $Zr_{47.5}Cu_{46.5}Al_5Co_1$ alloy; (e) SAED pattern taken from intervariant in (d); (f) Bright field image of $Zr_{47.5}Cu_{45.5}Al_5Co_2$ alloy; (g, h) SAED patterns taken from zones *M* and *A* in (f), respectively

increasing the content of Co. Thus, it can be seen that the martensitic transformation temperatures become low. These results are consistent with the previous investigations [19]. Although the amount of the martensite becomes small, all of them in the three alloys belong to Cm martensite. Rietveld refinement shows that at normal conditions in the intermetallic compound $Zr_{50}Cu_{50}$, *B*19′ and Cm martensite phases have 27% and 73% of the volume fraction correspondingly [11]. When the content of Al atom substituting for Zr atom is smaller than 9.375% (mole fraction), the austenite phase could form a martensite base structure during quenching or straining. While Al content is larger than 9.375% (mole fraction), it forms a superstructure [20]. In addition, the volume fraction of *B*19′ martensite becomes small due to the co-doping of Al and Co. So, it is more difficult to find *B*19′ martensite.

Martensitic transformation behavior of the ZrCuAlCo alloys is shown in Fig. 4. Only one-step transformation behaviors happen except for $Zr_{47.5}Cu_{46.5}Al_5Co_1$ alloy. It can be seen that two-step transformation behaviors are present in $Zr_{47.5}Cu_{46.5}Al_5Co_1$ alloy during reverse martensitic transformation (indicated by arrows). The results are occasionally found in forward martensitic transformation which attributed them to the transformation from *B*2 to *B*19′ and then to *Cm* phases on cooling progress [9]. The martensitic transformation temperatures of ZrCuAlCo alloys are shown in Table 1. As seen in Table 1, $Zr_{48}Cu_{47.5}Al_4Co_{0.5}$ alloy shows A_s=461 K and M_s=388 K, and transformation hysteresis (ΔH) is 73 K. With the addition of Co, the martensitic transformation temperature rapidly decreases. Increasing Al content induced a decrease in the martensitic transformation temperature until the Al content over 6% M_s remained almost constant [14]. The DSC results are fitted to the TEM results. When the addition of Co increases to 2%, the martensitic transformation temperature and the transformation hysteresis vary unobviously. This is likely to be resulted from the variation in the intrinsic factors, i.e. the increase in the unit-cell volume and the decrease in the electron concentration with increasing Co content because Co possesses small atomic radius and high electron concentration. The dependence of transformation temperature of ZrCu-based shape memory alloys on the number and concentration of valence electrons is analyzed.

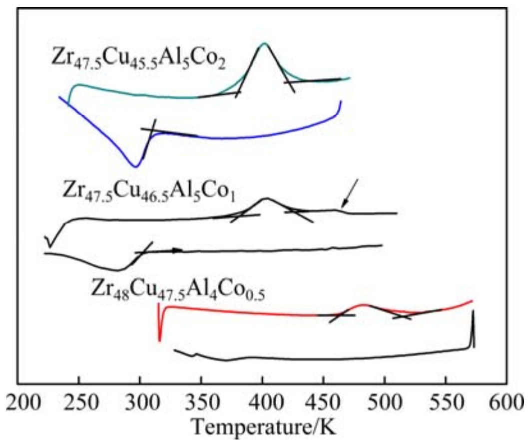

Fig. 4 DSC curves of ZrCuAlCo alloys

Table 1 Martensitic transformation temperatures of ZrCuAlCo alloys

Alloy	A_s/K	A_f/K	M_s/K	M_f/K	ΔH/K
$Zr_{48}Cu_{47.5}Al_4Co_{0.5}$	461	523	388	346	73
$Zr_{47.5}Cu_{46.5}Al_5Co_1$	376	432	305	238	71
$Zr_{47.5}Cu_{45.5}Al_5Co_2$	378	422	309	275	69

Figure 5 shows the tensile stress−strain curves of ZrCuAlCo alloys at room temperature. The elastic and plastic properties of ZrCuAlCo alloys by tensile tests are shown in Table 2. It can be seen that the compressive strength of ZrCuAlCo alloy is obviously enhanced by the addition of Co. Furthermore, the fracture strain is increased from 0.73% to 1.76%. The increase of the strength is mainly due to stress-induced martensitic transformation from a cubic $B2$ phase to a monoclinic martensite phase, which imparts an appreciable work-

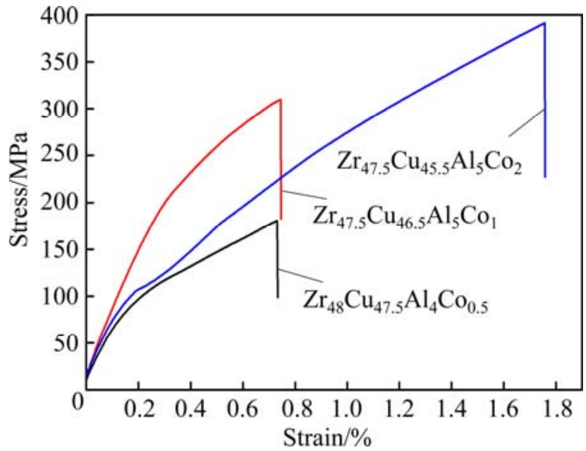

Fig. 5 Stress−strain curves of ZrCuAlCo alloys

Table 2 Elastic and plastic properties of ZrCuAlCo alloys by tensile tests

Alloy	Yield stress, $\sigma_{0.2}$/MPa	Maximum stress, σ_b/MPa	Fracture strain, δ/%
$Zr_{48}Cu_{47.5}Al_4Co_{0.5}$	136.25	181.08	0.73
$Zr_{47.5}Cu_{46.5}Al_5Co_1$	275.84	311.82	0.75
$Zr_{47.5}Cu_{45.5}Al_5Co_2$	367.95	392.59	1.76

hardening capability (the alloy becomes strong as it deforms). In order to clarify the fracture mechanism, the fracture morphologies of ZrCuAlCo alloys after tensile are observed, as shown in Fig. 6. The fracture type of Figs. 6(a) and (b) is similar to intergranular fracture. With the further increase of the Co content, the degree of ductile fracture accompanied with tearing ridges of $Zr_{47.5}Cu_{45.5}Al_5Co_2$ is increased. The fracture morphology with lots of brittle crystal particles is presented. In particular, lots of faults with tearing ridges appear, indicating that the ductile deformation is largely developed before fracture.

4 Conclusions

1) Compared with equiatomic binary ZrCu alloy, the co-doping of Al and Co in ZrCu alloy decreases both the martensitic transformation temperature and the martensitic transformation temperature hysteresis. Furthermore, the volume fraction of $B19'$ martensite becomes so little that it is rarely observed.

2) The Al and Co addition significantly refines the grains. The martensite plates become fine. The substructure of the ZrCuAlCo quaternary alloy is mainly (001) compound twin and the martensitic variants are (021) type I twins related.

3) The tensile fracture strength and strain obviously increase with the increase of Co content.

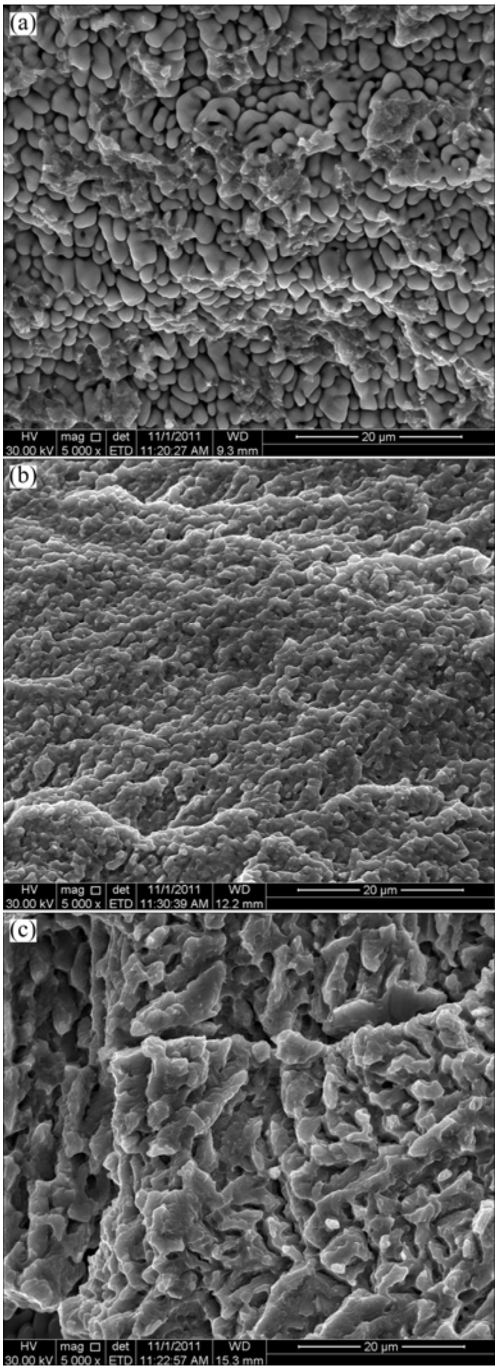

Fig. 6 SEM images of fracture surface of ZrCuAlCo alloys after tensile tests: (a) $Zr_{48}Cu_{47.5}Al_4Co_{0.5}$; (b) $Zr_{47.5}Cu_{46.5}Al_5Co_1$; (c) $Zr_{47.5}Cu_{45.5}Al_5Co_2$

References

[1] MA J, KARAMAN I, NOEBE R D. High temperature shape memory alloy [J]. International Materials Reviews, 2010, 55: 257−315.

[2] FIRSTOV G S, HUMBEECK J V, KOVAL Y N. High-temperature shape memory alloys some recent developments [J]. Materials Science and Engineering A, 2004, 378 : 2−10.

[3] MANJAIAH M, NARENDRANATH S, BASAVARAJAPPA S. Review on non-conventional machining of shape memory alloys [J]. Transactions of Nonferrous Metals Society of China, 2014, 24(1): 12−21.

[4] MENG Xiang-long, CAI Wei, ZHENG Yu-feng, ZHAO Lian-cheng. Phase transformation and precipitation in aged Ti−Ni−Hf high-temperature shape memory alloys [J]. Materials Science and Engineering A, 2006, 438−440: 666−670.

[5] MA Wen-jie, WANG Yu-ren, WEI Bing-chen, SUN Yu-feng. Microstructure and mechanical properties of Zr−Cu−A1 bulk metallic glasses [J]. Transactions of Nonferrous Metals Society of China, 2007, 17: 929−933.

[6] HOFMANN D C. Shape memory bulk metallic glass composites [J]. Science, 2010, 329: 1294−1295.

[7] PAULY S, LIU G, WANG G, KÜHN U, MATTERN N, ECKERT J. Microstructural heterogeneities governing the deformation of $Cu_{47.5}Zr_{47.5}Al_5$ bulk metallic glass composites [J]. Acta Materialia, 2009, 57: 5445−5453.

[8] WU Yuan, XIAO Yue-hua, CHEN Guo-liang, LIU C T, LU Zhao-ping. Bulk metallic glass composites with transformation mediated work-hardening and ductility [J]. Advanced Materials, 2010, 22: 2770−2773.

[9] YANG Bing, DU Yong, LIU Yong. Recent progress in criterions for glass forming ability [J]. Transactions of Nonferrous Metals Society of China, 2009, 19(1): 78−84.

[10] SCHRYVERS D, FIRSTOV G S, SEO J W, HUMBEECKT J V, KOVAL Y N. Unit cell determination in CuZr martensitic by electron microscopy and X-ray diffraction [J]. Scripta Materialia, 1997, 36: 1119−1125.

[11] FIRSTOV G S, HUMBEECKT J V, KOVAL Y N. Peculiarities of the martensitic transformation in ZrCu intermetallic compound-potential high temperature SMA [J]. Journal de Physique IV, 2001, 11: 481−486.

[12] KOVAL Y N, FIRSTOV G S, KOTKO A V. Martensitic transformation and shape memory effect in ZrCu intermetallic compound [J]. Scripta Metallurgica et Materialia, 1992, 27: 1611−1616.

[13] KOVAL Y N, FIRSTOV G S, DELAEY L, HUMBEECKT J V. The influence of Ni and Ti on the martensitic transformation and shape memory effect of the intermetallic compound ZrCu [J]. Scripta Metallurgica et Materialia, 1994, 31: 799−802.

[14] MENG Fan-qiang, TSUCHIYA K, YIN F X, YOKOYAMA Y. Influence of Al content on martensitic transformation behavior in $Zr_{50}Cu_{50-x}Al_x$ [J]. Journal of Alloys and Compounds, 2012, 522: 136−140.

[15] MENG Fan-qiang, TSUCHIYA K, YOKOYAMA Y. Influence of Ni on stability of martensitic transformation in $Zr50Cu_{50-x}Ni_x$ [J]. Journal of Alloys and Compounds, 2013. 577(S): s136−s140

[16] QIU Feng, SHEN Ping, LIU Chang, JIANG Qi-chuang. Effects of Ni addition on the microstructure and compressive deformation behavior in Zr−Cu−Ni martensitic alloys [J]. Materials and Design, 2012, 34: 143−147.

[17] JAVID F A, MATTERN N, PAULY S, ECKERT J. Effect of cobalt on phase formation, microstructure, and mechanical properties of $Cu_{50-x}Co_xZr_{50}$ (x=2, 5, 10, 20 at. pct) alloys [J]. Metallurgical and Materials Transactions A, 2012, 43: 2631−2636.

[18] BIFFI C A, ALBISETTI A F, TUISSI A. CuZr based shape memory alloys: Effect of Cr and coon the martensitic transformation [J]. Materials Science Forum, 2013, 738−739: 167−171.

[19] JAVID F A, MATTERN N, PAULY S, ECKERT J. Martensitic transformation and thermal cycling effect in Cu–Co–Zr alloys [J]. Journal of Alloys and Compounds, 2011, 509(S): s334−s337.

[20] QIU Feng, SHEN Ping, LIU Tao, LIN Qiao-li, JIANG Qi-chuan. Electronic structure and phase stability during martensitic transformation in Al-doped ZrCu intermetallics [J]. Journal of Alloys and Compounds, 2010, 491: 354−358.

Al 和 Co 的添加对 ZrCu 基形状记忆合金的马氏体相变和显微结构的影响

高卫红，孟祥龙，蔡 伟，赵连城

哈尔滨工业大学 材料科学与工程学院，哈尔滨 150001

摘 要：研究 Al 和 Co 元素掺杂的 ZrCu 基形状记忆合金的马氏体相变。结果表明，Al 和 Co 的添加降低了马氏体相变温度，同时降低了马氏体相变温度滞后。TEM 结果显示，*Cm* 结构的马氏体为优先形成相。在 ZrCuAlCo 合金中内部马氏体变体呈(021) I 型孪晶关系，然而主要的亚结构呈(001)复合孪晶关系。随着 Co 含量的增加，拉伸断裂强度和应变显著提高。

关键词：ZrCu 基合金；形状记忆合金；马氏体相变；显微结构

(Edited by Xiang-qun LI)